METHODS AND AHE AGE SELECTION

Apatite grains have been isolated following classical density and magnetic methods and then picked under a binocular lens. AHe analyses have been performed at the Orsay/IDES low temperature thermochronology laboratory (University of Paris Sud XI, France).

AHe ages have been measured on carefully selected apatite grains, which have been measured along the three axes. Several replicates have been analyzed per sample. Sphere equivalent radius, grain weight and ejection factors have been determined using the Monte Carlo simulation of Ketcham et al. (2011), see Table DR2. Apatite grains were placed into platinum baskets and heated twice using a diode laser at 1030 ± 50 °C during 5 minutes, to allow total He degassing and to check the presence of He trapped in small inclusions. Sample presenting a second re-heating gas level higher than the blank level are not presented in this study. The ^{4}He content was determined by comparison with a ~1-2×10^{-7} cc STP ^{3}He spike. After He extraction, platinum baskets were placed into single-use polypropylene vials. Apatite grains were dissolved one hour at 90°C in a 50µl HNO_3 solution containing a known content of ^{235}U and ^{230}Th, and then filled with 1 ml of ultrapure MQ water. The final solution was measured for U and Th concentrations by quadrupole ICP-QMS using a series II CCT Thermo-Electron at LSCE (Gif/Yvette; France). The analysis was calibrated using internal and external age standards. Mean AHe ages of 16.6 ± 1.1 Ma and 31.4 ± 1.4 Ma have been measured for the Limberg tuff and Durango yellow apatite respectively, which are in agreement with literature data, i.e. 16.8 ± 1.1 Ma (Kraml et al., 2006) and 31.4 ± 0.2 Ma (McDowell et al., 2005). Because the grain sizes were really small in some cases, error propagation taking into account the size in addition to standard reproducibility has been calculated. The error on AHe age at 1σ is estimated to be 7% for the biggest grains (Rs=63 µm) and increases up to 37% for the smallest grains (Rs=23 µm).

The Saharan climate is warm, summer noon temperatures of up to 50°C are common in the region. In order to ensure that climate did not affect He retention in the collected samples, we ran heating simulations. Our calculations show that heating of 45°C during 0.1 Ma results in diffusion of 3.8% He, for a 20 µm sphere equivalent radius apatite. For a radius of 40µm, He loss is estimated to be 1.6%. As these variations are clearly less than final uncertainties, we neglected the climate effect, as already proposed by Wolf et al. (1998).

The final He, U-Th contents and He ages are reported in Table DR2. Like other studies on cratonic areas (see for example: Green and Duddy, 2006; Hansen and Reiners, 2006; Gautheron et al., 2009), AHe ages of this study are scattered. Replicates yielding AHe age either older by more than 50 % of the mean will not be taken into consideration. They are interpreted as induced

by ^{4}He contamination due to α-implantation, small undetected U-Th-rich inclusions, and diffusion due to damage and annealing processes (Gautheron et al., 2009). The cut off at 50% is taken as a larger limit of external processes affecting AHe age, a limit which is higher than general F_T overcorrection for standard kinetic and damage model, α-implantation (Gautheron et al., 2012). In addition, some replicates yield AHe age higher than their sample mean value at more than 30% and yield different Th/U ratios. We propose, using these criteria, to exclude these replicates (marked with the † symbol in Table DR2).

AHe age simulations (Figure S1) were carried out using our 3D diffusion code (Gautheron and Tassan-Got, 2010), and with a non-constant He diffusion behavior taking into account alpha-damage production and annealing (Gautheron et al., 2009). We consider a thermal history (Figure S1C) with a slow cooling during the Jurassic, a 20°C stage during the Lower Cretaceous, a heating stage from 100 to 40 Ma with variable burial peak temperature, and a rapid cooling representative of the Eocene exhumation stage. Simulated AHe age are reported in function of 60-40 Ma peak temperature (from 20 to 120 °C), for representative values of 1, 5, 10, 50 and 100 ppm for effective uranium content (eU=U+0.24Th in ppm) with a 50µm sphere equivalent radius (Figure S1A); as well as 30, 50, 70 and 90 µm sphere radius with 10 ppm eU content (Figure S1B). These simulations show that AHe age dispersion is maximal (with AHe ages ranging from 40 to 180 Ma) in the 60-80°C temperature interval. Given the strong dispersion in the samples measurements, it is thus reasonable to consider that the temperature reached by the samples before the Eocene exhumation stage has not been lower than ~60°C nor exceeded ~80°C.

TABLE DR1. SAMPLES LOCATION, DESCRIPTION AND (U-Th)/He AGE

Sample	Lat (°N)	Long (°E)	Alt (m)	Description
SILET-ALG				
ALG2	22.57	4.38	699	Granodiorite
ALG3	22.48	4.49	707	Granodiorite
ALG4	22.54	4.56	722	Granodiorite
ARAK-FRZ				
FRZ1	25.72	3.51	625	Cambro-Ordovician sandstone
AIR-BLN				
BLN12	17.58	9.59	671	Rhyolite
BLN400	19.57	8.62	802	Mylonitic metatonalite
IN TEDEINI – TIN ZAOUATENE-TZA				
TZA14	23.93	4.49	827	Imelehatene granite
TZA28	24.03	4.38	754	Tidjelamine granite
TZA182	25.07	4.03	834	Mouydir granodiorite
TZA204	24.68	4.73	912	Tesnou granite
TIN GHORAS-ARO				
ARO113	23.73	8.49	1037	Tin Ghoras granite
ARO108	23.73	8.49	1037	Tin Ghoras granite
OUNANE-TOD				
TOD17	24.95	7.27	1341	Tisselliline granite
TOD27	25.11	7.34	1372	Ounane granodiorite
TOD30	25.00	7.29	1416	Tisselliline granite
IN TOUNINE-IT				
IT05	22.77	5.7	1523	In Tounine granite
IT22	22.75	5.73	1537	In Tounine granite

TABLE DR2. APATITE (U-Th)/He DATA

Name	Nb.	Rs (µm)	Weight (µg)	F_T	^{4}He (ncc/g)	U (ppm)	Th (ppm)	Th/U	eU (ppm)	Age (Ma)	Age c. (Ma)*
ALG2-1	2546	42.9	2.3	0.70	81.7	17.5	44.3	2.5	28.2	24.1	34.5 ± 3.2
ALG2-2	4937	28.8	0.62	0.574	151.3	42.5	122.5	2.9	71.9	17.5	30.5 ± 2.4
ALG2-3	4939	37.1	1.62	0.678	88.3	17.8	65.1	3.6	33.5	22	32.4 ± 2.6
ALG2-4	4941	34.7	1.03	0.648	154.3	27	48.4	1.8	38.6	33.2	51.3 ± 4.1
ALG2-5	4945	49.1	2.03	0.714	160.3	25.7	85.4	3.3	46.2	28.9	40.5 ± 3.2
ALG2-6	4947	41.1	1.66	0.7	161.2	24.3	71.9	3	41.5	32.3	46.2 ± 3.7
ALG2-8	4951	36.6	1.49	0.678	191.0	21.5	84.4	3.9	41.7	38.1	56.3 ± 4.5
ALG2-B	2039	60.0	4.8	0.83	131.8	32.5	21.8	0.7	37.8	28.9	34.9 ± 2.4
ALG2-C	2041	46.8	3.7	0.72	61.0	11.7	31.6	2.7	19.3	26.3	36.4 ± 2.8
ALG2-D	2043	50.2	4.6	0.78	136.4	23.0	28.4	1.2	29.8	38.0	48.9 ± 3.4
ALG3-1	2548	56.0	6.4	0.77	134.6	17.0	29.8	1.8	24.2	46.3	60.4 ± 4.2
ALG3-2	2550	49.5	8.3	0.75	206.4	34.5	55.0	1.6	47.7	35.9	48.2 ± 3.4
ALG3-3	2594	44.8	4.1	0.72	187.2	36.2	67.5	1.9	52.4	28.3	39.4 ± 3.1
ALG3-5	4955	43.2	1.77	0.677	117.3	26.8	45.5	1.7	37.7	25.8	38.2 ± 3.1
ALG3-6	4957	36.5	1.13	0.624	189.0	52.5	81.4	1.6	72	21.8	34.9 ± 2.8
ALG3-7	4962	44	2.4	0.709	133.4	30.9	52.9	1.7	43.6	25.4	35.9 ± 2.9
ALG3-B	2025	47.0	3.8	0.76	108.0	25.8	37.8	1.5	34.8	25.7	33.9 ± 2.4
ALG3-E	2035	44.0	2.0	0.72	333.6	55.3	97.5	1.8	78.7	35.2	49.0 ± 3.8
ALG4-1	2596	51.4	6.9	0.75	270	24.4	11.1	0.5	27.1	82.8	110.6 ± 7.7†
ALG4-2	2598	41.9	1.8	0.70	289.6	19.9	55.1	2.8	33.1	72.8	104.0 ± 9.9†
ALG4-3	2600	29.0	0.9	0.57	129.8	34.4	45.2	1.3	45.2	23.8	41.8 ± 9.4

FRZ1-2	4047	28.9	0.85	0.60	39.1	4.0	19.5	1.3	51.9	37.5	62.5 ± 11.8
FRZ1-3	4049	28.1	0.74	0.57	342.9	9.2	4.0	0.4	10.2	278.3	484.8 ± 106.3†
FRZ1-5	4055	36.6	1.28	0.66	49.0	4.2	10.1	2.4	6.7	61.2	93.5 ± 12.3
FRZ1-6	4057	55.1	4.08	0.77	120.2	1.6	4.3	2.7	2.6	381.3	493.9 ± 34.6†
FRZ1-7	4059	89.9	15.13	0.86	22.2	0.7	1.5	2.3	1.0	181.7	210.8 ± 14.8†
BLN12-2-2	4175	31.6	1.26	0.57	111.6	4.8	41.0	8.5	14.9	63.5	111.0 ± 24.6†
BLN12-2-4	4179	50.5	3.25	0.75	259.9	31.3	15.7	0.5	35.1	61.4	82.3 ± 4.8
BLN12-2-5	4181	36.6	1.49	0.68	250.7	14.7	28.4	1.9	21.7	96.8	142.8 ± 15.8†
BLN12-2-6	4400	38.5	1.07	0.65	35.0	4.0	53.0	13.2	17.0	17.5	27.1 ± 3.8
BLN12-2-7	4402	58.3	4.45	0.80	52.9	3.3	14.6	4.4	6.8	65.1	81.9 ± 5.7
BLN12-2-8	4404	34.7	1.13	0.64	143.3	4.7	35.0	7.4	13.3	91.4	142.2 ± 20.4†
BLN12-2-10	4408	33.9	0.99	0.64	277.2	3.4	27.1	8.0	10.0	233.8	363.6 ± 52.2†
BLN400-2-1	4185	31.3	0.62	0.63	56.1	12.9	33.6	2.6	21.1	22.3	35.5 ± 5.7
BLN400-2-2	4187	29.0	0.73	0.55	161.1	36.4	29.4	0.8	43.6	30.7	56.2 ± 14.2
BLN400-2-3	4189	50.4	3.52	0.75	130.7	20.8	4.8	0.2	21.9	49.3	66.1 ± 4.6
BLN400-2-5	4582	34.3	0.92	0.65	40.8	16.7	17.9	1.1	21.1	16.1	24.9 ± 3.5
BLN400-2-7	4587	42.3	2.09	0.70	102.6	7.2	9.2	1.3	9.5	90.5	128.8 ± 11.6†
BLN400-2-9	4591	27.5	0.56	0.60	43.5	30.2	51.9	1.7	42.9	8.5	14.1 ± 2.6
BLN400-2-10	4593	31.7	0.7	0.64	147.8	67.3	53.0	0.8	80.3	15.3	24.1 ± 3.7
TZA14-1	4443	38.8	2.31	0.68	65.1	6.5	20.3	3.1	11.4	47.9	70.5 ± 7.8
TZA14-2	4423	46.4	4.02	0.73	395.0	18.6	63.4	3.4	34.1	97.3	133.9 ± 9.6†
TZA14-3	4425	63.1	6.88	0.82	61.9	12.8	23.7	1.8	18.6	27.8	34.1 ± 2.4
TZA14-4	4427	50.1	3.56	0.77	127.9	16.3	53.2	3.3	29.4	36.6	47.9 ± 3.4
TZA14-5	4429	35.3	0.89	0.68	651.9	115.1	286.3	2.5	185.3	29.5	43.5 ± 4.8
TZA28-1	3852	30.1	1.0	0.60	345.8	28.8	108.7	3.8	45.7	52.5	87.2 ± 16.3
TZA28-2	3856	42.8	2.0	0.71	307.9	64.6	20.2	0.3	46.2	36.7	52.0 ± 4.6
TZA28-3	3860	30.5	1.0	0.60	628.4	64.3	42.1	0.7	61.9	70.0	116.3 ± 21.7†
TZA28-4	4231	44.4	2.95	0.71	727.9	84.7	21.1	0.2	89.9	67.1	94.6 ± 8.1
TZA28-6	4437	28.3	0.64	0.60	282.2	172.9	64.4	0.4	188.7	12.4	20.6 ± 3.8
TZA28-7	4439	46.2	2.5	0.77	346.8	65.6	77.6	1.2	84.6	34.2	44.6 ± 3.1
TZA28-8	4441	29.4	0.8	0.60	1252.7	91.4	50.1	0.5	103.7	100.3	166.3 ± 30.9†
TZA28-9	4467	59.2	5.09	0.81	215.5	39.0	50.1	1.3	51.3	35.0	43.2 ± 3.0
TZA182-1	3847	29.2	1.7	0.57	493.9	18.0	37.5	2.1	21.6	151.8	267.4 ± 60.6†
TZA182-2	3849	30.1	1.0	0.60	193.1	26.9	115.2	4.3	77.8	29.5	49.0 ± 9.2
TZA182-3	3852	24.2	1.7	0.50	182.7	10.6	42.8	4.0	20.9	73.0	145.0 ± 45.4†
TZA182-9	4818	31.5	0.74	0.68	240.1	14	68	4.88	30.3	66.1	92.5 ± 14.4
TZA182-10	4820	46.2	2.17	0.74	331.6	19.2	40	2.18	28.8	95.5	129.6 ± 40.1†
TZA182-11	4935	42.3	2.21	0.703	570.4	19.4	51.9	2.7	31.9	148.8	211.6± 16.9†
TZA204-1	3873	56.9	4.6	0.77	19.8	17.5	15.3	0.9	14.9	7.8	10.1 ± 0.7
TZA204-2	3875	50.7	3.4	0.70	35.8	2.4	19.5	8.0	5.0	42.1	59.8 ± 5.3
TZA204-3	3877	50.9	6.2	0.81	38.5	4.0	18.5	4.6	7.5	38.0	46.6 ± 3.3
TZA204-4	3879	48.3	5.4	1.05	138.8	7.6	33.6	4.4	12.7	74.0	70.3 ± 4.9
TZA204-5	3881	45.6	2.3	0.80	98.4	15.9	94.9	6.0	32.4	21.2	26.8 ± 1.9
ARO113-1	3837	42.0	3.0	0.67	639.1	12.4	135.8	10.9	36.3	118.7	178.4 ± 21.8†
ARO113-2	3841	31.4	1.2	0.59	467.8	143.9	1556.7	10.8	397.0	7.6	12.9 ± 2.6
ARO113-3	3843	42.9	1.6	0.73	47.2	15.1	47.8	3.2	18.2	14.8	20.4 ± 1.5
ARO113-4	3845	23.3	0.4	0.47	551.1	44.7	118.6	2.7	52.2	62.7	132.3 ± 47.1†
ARO108-5	4459	35.5	1.24	0.62	338.1	82.1	119.7	1.5	111.4	25.3	40.7 ± 6.7
ARO108-6	4463	39.5	1.42	0.71	332.7	11.9	42.3	3.5	22.3	125.4	175.8 ± 14.5†
ARO108-7	4465	27.1	0.46	0.57	371.1	20.4	92.2	4.5	43.0	72.8	128.8 ± 29.7†
TOD17-1	4469	29.8	0.78	0.58	394.1	14.9	84.0	5.6	35.5	93.7	161.6 ± 34.3†
TOD17-3	4471	28.8	0.62	0.58	309.2	38.7	153.6	4.0	76.4	34.1	59.3 ± 12.9
TOD17-5	4475	28.8	0.62	0.58	109.5	14.9	67.9	4.6	31.5	29.3	51.0 ± 11.1
TOD17-6	4477	27.5	0.56	0.60	64.2	6.1	55.7	9.1	19.8	27.5	45.7 ± 8.5
TOD17-7	4479	26.6	0.48	0.60	86.4	7.8	69.2	8.9	24.7	29.7	49.2 ± 9.1
TOD17-8	4483	31.1	0.91	0.56	379.5	84.5	131.3	1.6	116.7	27.2	48.3 ± 11.2
TOD17-2	4493	28.8	0.62	0.58	188.3	29.4	108.5	3.7	56.0	28.3	49.2 ± 10.7
TOD17-9	4500	31.8	0.67	0.58	127.4	110.4	82.5	0.7	130.6	8.1	13.9 ± 2.9

TOD17-11	4504	22.9	0.43	0.50	143.9	80.7	519.2	6.4	207.9	5.9	11.8 ± 3.8
TOD27-1	4552	37.7	1.33	0.63	40.1	80.6	48.5	0.6	92.4	3.6	5.7 ± 0.9
TOD27-2	4554	42.3	2.1	0.68	10.8	2.7	16.6	6.2	6.8	22.2	32.7 ± 3.6
TOD27-3	4558	22.9	0.43	0.47	26.3	10.1	38.2	3.8	19.4	11.4	24.2 ± 8.7
TOD27-4	4560	34.8	0.83	0.61	65.3	187.3	18.3	0.1	191.8	2.8	4.6 ± 0.8
TOD27-5	4562	23.0	0.7	0.46	47.2	17.2	79.4	4.6	36.7	10.8	23.3 ± 8.6
TOD27-8	4576	36.0	1.46	0.65	55.2	10.6	23.0	2.2	16.2	28.5	43.6 ± 5.8
TOD27-10	4580	32.9	0.87	0.64	32.0	9.0	39.6	4.4	18.7	14.4	22.6 ± 3.3
TOD30-2	4507	26.6	0.48	0.56	714.9	77.0	217.5	2.8	130.3	46.0	82.0 ± 19.3[†]
TOD30-3	4512	20.7	0.24	0.50	951.0	80.7	517.5	6.4	207.5	38.8	78.3 ± 25.4[†]
TOD30-4	4514	25.1	0.43	0.55	99.4	93.9	68.4	0.7	110.7	7.5	13.5 ± 3.4
IT05-1	3863	32.6	2.2	0.64	1493.4	39.1	311.5	8.0	85.3	109.6	170.0 ± 24.1[†]
IT05-2	3865	57.5	4.9	0.77	53.9	4.4	32.2	7.2	8.6	36.9	48.0 ± 3.4
IT05-3	3867	50.3	3.8	0.77	2257.8	31.9	215.1	6.7	68.8	225.7	294.6 ± 20.6[†]
IT05-4	3869	23.3	0.4	0.47	2479.4	350.0	995.2	2.8	420.6	35.0	74.6 ± 27.0
IT05-5	3871	47.9	2.8	0.76	911.8	43.0	509.7	11.9	149.6	46.1	60.4 ± 4.2
IT05-6	4516	32.9	0.87	0.68	141.8	13.8	118.1	8.6	42.7	28.1	41.4 ± 4.6
IT05-7	4518	30.5	1.04	0.60	123.1	3.7	39.4	10.5	13.4	78.0	129.5 ± 24.2[†]
IT05-10	4526	36.6	1.49	0.68	963.5	30.0	263.4	8.8	94.6	86.4	127.4 ± 14.1[†]
IT05-11	4528	49.8	3.02	0.75	109.8	8.2	71.6	8.7	25.7	36.2	48.5 ± 3.4
IT22-1	4532	51.8	3.36	0.79	574.7	36.8	72.7	2.0	54.6	88.1	111.0 ± 7.8
IT22-2	4536	43.4	2.44	0.71	326.8	7.4	43.6	5.9	18.1	152.9	216.8 ± 19.2[†]
IT22-3	4538	30.1	0.96	0.60	210.8	6.6	110.9	16.8	33.8	53.2	88.3 ± 16.5
IT22-4	4540	42.9	2.28	0.68	278.3	61.9	22.0	0.4	67.3	34.3	50.3 ± 5.5
IT22-5	4542	36.6	1.49	0.66	661.5	11.5	82.1	7.1	31.6	177.1	270.4 ± 35.7[†]
IT22-8	4550	49.0	2.78	0.72	407.1	117.9	95.1	0.8	141.2	24.0	33.4 ± 2.7

*(U-Th)/He age corrected from alpha ejection, with analytical incertitude at 1 sigma (see text).

[†]Excluded higher result (see text).

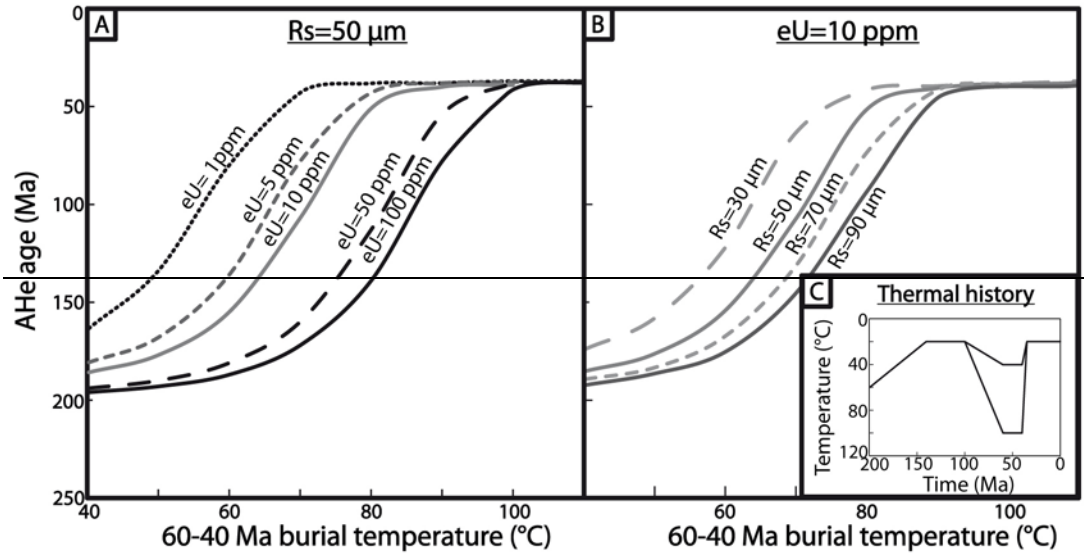

Figure DR1: Simulated AHe age evolution as a function of the 60-40 Ma burial temperature for (A) several effective uranium content (eU=1, 5, 10, 50 and 100 ppm) and (B) several crystal sizes (equivalent sphere radius of 30, 50, 70 and 90 µm) for a (C) representative thermal history. Age simulations were done using non-constant He diffusion code of Gautheron et al. (2009), Gautheron and Tassan-Got (2010). See supplementary materials text for details.

REFERENCES

Gautheron, C.E., Tassan-got, L., Barbarand, J. and Pagel, M., 2009, Effect of alpha-damage annealing on apatite (U-Th)/He thermochronology: Chemical Geology, v. 266, p.166-179.

Gautheron, C. and Tassan-got, L., 2010, A Monte Carlo approach to diffusion applied to noble gas/helium thermochronology: Chemical Geology, v. 273, p. 212-224.

Gautheron, C., Tassan-got, L., Ketcham, R.A. and Dobson, K.J., 2012, Accounting for long alpha-particle stopping distances in (U-Th-Sm)/He geochronology: 3D modeling of diffusion, zoning, implantation, and abrasion: Geochemica Cosmochimica Acta, v. 96, p. 44-56.

Green, P.F. and Duddy, I.R., 2006, Interpretation of apatite (U-Th)/He ages and fission track ages from cratons: Earth and Planetary Science Letters, v. 244, p.541-547.

Hansen, K. and Reiners, P.W., 2006, Low temperature thermochronology of the southern East Greenland continental margin: Evidence from apatite (U-Th)/He and fission track analysis and implications for intermethod calibration: Lithos, v. 92, p.117-136.

Ketcham, R.A., Gautheron, C. and Tassan-got, L., 2011, Accounting for long alpha-particle stopping distances in (U-Th-Sm)/He geochronology: refinement of the baseline case: Geochimica et Cosmochimica Acta, v. 75, p.7779-7791.

Kraml, M., Pik, R., Rahn, M., Selbekk, R., Carignan, J. and Keller, J., 2006, A new multi-mineral age reference material for 40Ar/39Ar, (U-Th)/He and fission track dating methods: The Limberg t3 tuff: Geostandards and Geoanalytical Research, v. 30, p.73-86.

McDowell, F.W., McIntosh, W.C. and Farley, K.A., 2005, A precise 40Ar-39Ar reference age for the Durango apatite (U-Th)/He and fission-track dating standard: Chemical Geology, v. 214, p.249-263.

Wolf, R.A., Farley, K.A. and Kass, D.M., 1998, Modeling of the temperature sensitivity of the apatite (U-Th)/He thermochronometer: Chemical Geology, v. 148, p.105-114.